Equation of state and conductivities of dense hydrogen plasmas near the metal-insulator transition

Shigenori Tanaka
Department of Physics, University of Tokyo, Bunkyo-ku, Tokyo, Japan

Xin-Zhong Yan
Institute of Physics, Chinese Academy of Science, Beijing 100080, People's Republic of China

Setsuo Ichimaru
Department of Physics, University of Tokyo, Bunkyo-ku, Tokyo, Japan
and Institute for Theoretical Physics, University of California, Santa Barbara, California 93106
(Received 27 December 1989)

Strong correlations between electrons and ions in hydrogen plasmas near metal-insulator boundaries are analyzed through an integral equation approach, which adopts the hypernetted-chain (HNC) approximation for the classical ion-ion correlation and the modified convolution approximation (MCA) for the quantum-mechanical electron-electron and electron-ion correlations. The resulting HNC MCA equations are solved self-consistently. The correlation functions and the equation of state thus calculated reveal the emergence of "Rydberg states" in the metallic phase near the metal-insulator boundaries, which acts to reduce the electric and thermal conductivities. Parametrized formulas for the equation of state and the conductivities are presented.

I. INTRODUCTION

In an earlier series of investigations[1-4] Ichimaru, Mitake, Tanaka, and Yan (IMTY) developed a strong-coupling theory of dense hydrogen plasmas appropriate to the interior of the main-sequence stars and to final stages of inertial-confinement fusion plasmas. In such a dense plasma, the strong Coulomb and exchange coupling between the charged particles beyond the random-phase approximation[1,5] (RPA) becomes essential. In the density-response formalism, on which the IMTY theory is based, such a strong-coupling effect can be treated rigorously in terms of the local-field corrections[1] (LFC's).

When the density and/or temperature of the plasma are lowered toward the conditions for the onset of pressure and/or thermal ionization, the Coulomb coupling between the electrons and the ions becomes particularly pronounced; a trend toward an incipient formation of bound pairs (i.e., neutral atoms) should be revealed in the features of the electron-ion correlations. A major shortcoming of the IMTY theory lies in its inaccuracy in treating such an effect of strong electron-ion coupling as the plasma approaches the metal-insulator boundaries. They approximately expressed the joint distributions between electrons and ions in terms of linear response of the electrons against the ions; as a consequence, the LFC between electrons and ions vanished identically in their calculations. The predicted equation of state[3] (EOS) did not show a tendency toward incipient bound pairs; the calculated values[4] of the conductivities remained relatively high near the metal-insulator boundaries.

In this paper, we develop a strong-coupling theory of dense hydrogen plasmas applicable in the vicinity of the metal-insulator boundaries (see Fig. 1). Strong Coulomb and exchange correlations are analyzed through an integral equation approach, which adopts the hypernetted-chain (HNC) approximation[1] for the classical ion-ion correlations and the modified-convolution approximation[6] (MCA), justified both in the classical plasmas[7] and in the quantum electron liquids,[8] for the quantum-mechanical electron-electron and electron-ion correlations. The resulting HNC MCA equations are solved self-consistently for the structure factors and the LFC's. The EOS thus calculated reveals the emergence of "Rydberg states" in the metallic phase, implying physically an approach toward an insulator phase. The Rydberg states are found to modify the electron-ion correlations remarkably and act to reduce the electric and thermal conductivities. Parametrized formulas for the EOS and the conductivities are provided for a practical application.

The strong-coupling effects in dense plasmas have been studied theoretically by a number of investigators.[1] Earlier in 1982, Dharma-wardana and Perrot[9] (referred to as DP) presented a density-functional theory of hydrogen plasmas. In this theory, the ion-ion correlations were analyzed in the HNC approximation. The electron-electron correlations, however, were treated in the density-functional formalism[10] with the local-density approximation (LDA); essential spatial-dispersion (i.e., wave-number-dependent) effects in the electron-electron LFC were thus ignored. Furthermore, they neglected the contributions of exchange-correlation potential altogether in their LDA treatment of the electron-ion correlations; no LFC effects were therefore retained. More recently,[11] these authors applied analogous correlation calculations to the electric resistivity in hot dense plasmas, where electron scattering against ions beyond the Born approximation was treated through phase-shift analyses. Whenever feasible, the results of the present study will be compared with those of DP, although degrees of approximations involved are significantly different.

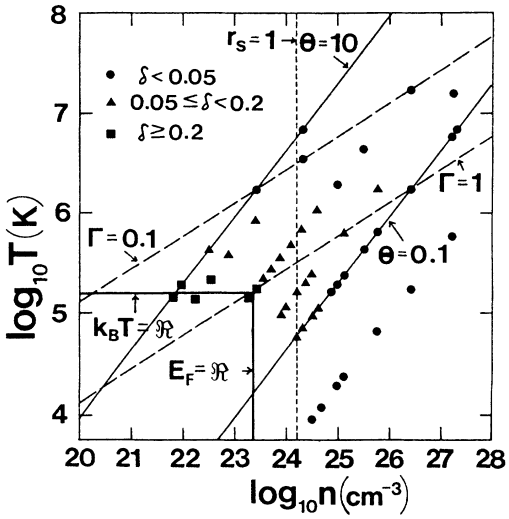

FIG. 1. Various parameters on the number density vs temperature plane for hydrogen plasma. See the text for definition of Γ, r_s, Θ, and δ.

II. METAL-INSULATOR BOUNDARIES

We consider a hydrogen plasma at temperature T with n electrons and n ions (protons) in a unit volume. The Coulomb-coupling parameter[1] for such a plasma is

$$\Gamma=\frac{e^2}{ak_BT}\ , \tag{1}$$

where $a=(3/4\pi n)^{1/3}$ is the ion-sphere radius. The dimensionless density parameter and degeneracy parameter for the electrons are

$$r_s=ame^2/\hbar^2\ , \tag{2}$$

$$\Theta=k_BT/E_F\ , \tag{3}$$

where $E_F=\hbar^2k_F^2/2m$ is the Fermi level of the electrons in the ground state with $k_F=(3\pi^2n)^{1/3}$. In Fig. 1 we show relative magnitude of those parameters on the n-T plane.

We take the condition for pressure ionization in hydrogen approximately as

$$E_F=\mathcal{R}\ , \tag{4}$$

where $\mathcal{R}=me^4/2\hbar^2=13.6$ eV, the ionization energy of a hydrogen atom in the ground state. Analogously the condition for thermal ionization is taken approximately as

$$k_BT=\mathcal{R}\ . \tag{5}$$

Relations (4) and (5) are likewise displayed in Fig. 1. Hydrogen is in an ionized, metallic state, when $E_F>\mathcal{R}$ or $k_BT>\mathcal{R}$.

For an isolated hydrogen atom in the ground state, the value of the joint probability function between an electron and an ion at $r=0$ is

$$g_{12}^0(0)=\frac{1}{n}|\psi_{1s}(0)|^2=\tfrac{4}{3}r_s^3\ , \tag{6}$$

where $\psi_{1s}(r)$ is the wave function for a $1s$ electron. The electron-ion interaction energy in such an atom is $-2\mathcal{R}$, so that

$$E_{12}^0/Nk_BT=-\tfrac{1}{2}(9\pi/4)^{2/3}\Theta\Gamma^2\ . \tag{7}$$

As hydrogen plasmas approach the boundaries, (4) and (5), in Fig. 1, coupling between electrons and ions becomes so pronounced that features resembling (6) and (7) of a bound state may emerge in their correlation characteristics. Such will be called Rydberg states in hydrogen plasma, with an implication to incipient bound states.

III. HNC SCHEME

We investigate the interparticle correlations, EOS, and transport properties in dense hydrogen plasmas through the solution to a set of integral equations in the density-response formalism[1] with the HNC approximation and MCA. The wave-number and frequency-dependent density-density response functions $\chi_{\mu\nu}(\mathbf{k},\omega)$ are thus expressed explicitly in terms of the free-particle polarizabilities $\chi_\mu^{(0)}(k,\omega)$ and the LFC's $G_{\mu\nu}(k,\omega)$. The subscripts μ and ν are introduced here to distinguish between the particle species; 1 is reserved for the electrons and 2 for the ions. For generality we designate the charge number by Z_μ and assume the macroscopic charge neutrality: $\sum_\mu Z_\mu n_\mu=0$.

In the density-response formalism, the LFC's play major parts in describing the strong Coulomb- and exchange-coupling effects beyond the RPA. Since $\chi_\mu^{(0)}(k,\omega)$ can be calculated at an arbitrary degeneracy,[1,12] the structure factors $S_{\mu\nu}(k)$ and the joint probability functions (i.e., the radial distribution functions, RDF's) are formulated exactly through the fluctuation-dissipation theorem[1] once the LFC's are known. Thermodynamic functions and transport coefficients then follow through a standard procedure.[1]

We approach the strong Coulomb-correlation effects between ions in the HNC scheme, assuming that the ions obey the classical statistics. Although the derivation of HNC equations is a canonical subject in the theory of simple liquids,[1,12] we briefly retrace it here, so that an explicit expression for $G_{22}(k)$ is obtained in the HNC approximation.

To begin, let us set the position of one of the ions at the origin $\mathbf{r}=\mathbf{0}$, and consider the spatial distributions of other ions, $n_2(r)$, and of the activities,[13] $z_\mu(r)$, which may be written as

$$n_2(r)=n_2g_{22}(r)=n_2+n_2h_{22}(r)\ , \tag{8}$$

$$z_\mu(r)=\exp[\alpha_\mu-v_{2\mu}(r)/k_BT]\ . \tag{9}$$

Here, α_μ denotes the normalized chemical potential, $v_{2\mu}(r)$ refers to the potential between the ion and a μ-species particle, and $h_{\mu\nu}(r)=g_{\mu\nu}(r)-1$ is the pair-correlation function between the μ and ν species.

The direct correlation functions are then calculated in terms of the functional derivatives as[13]

$$c_{\mu\nu}(\mathbf{r},\mathbf{r}')=\frac{\delta}{\delta n_\nu(\mathbf{r}')}\ln[n_\mu(\mathbf{r})/z_\mu(\mathbf{r})]$$
$$=\frac{1}{n_\mu}\delta_{\mu\nu}\delta(\mathbf{r}-\mathbf{r}')-\frac{\delta}{\delta n_\nu(\mathbf{r}')}\ln z_\mu(\mathbf{r}) \quad (10)$$

and are connected with the pair-correlation functions $h_{2\nu}(\mathbf{r},\mathbf{r}')$ via the Ornstein-Zernike relations[13]

$$h_{2\nu}(\mathbf{r},\mathbf{r}')=c_{2\nu}(\mathbf{r},\mathbf{r}')+\sum_\lambda\int d\mathbf{r}_1 n_\lambda h_{2\lambda}(\mathbf{r},\mathbf{r}_1)c_{\lambda\nu}(\mathbf{r}_1,\mathbf{r}') . \quad (11)$$

The HNC approximation consists in expanding $\ln[n_2(r)/z_2(r)]$ to the first order in $n_\mu h_{\mu 2}(r)$, so that

$$\ln[n_2(r)/z_2(r)]\approx\ln n_2-\alpha_2+\sum_\mu\int d\mathbf{r}' n_\mu h_{\mu 2}(\mathbf{r}')c_{2\mu}(\mathbf{r},\mathbf{r}') . \quad (12)$$

With the aid of Eqs. (8), (9), and (11), Eq. (12) is transformed into

$$g_{22}(r)=\exp[-v_{22}(r)/k_BT+h_{22}(r)-c_{22}(r)] , \quad (13)$$

an HNC equation for the ion-ion correlation.

The set of HNC equations, (11) and (13), can be rewritten exactly in a form which accommodates the electron-screened ion-ion potential[1,2] and thereby the LFC's. For this purpose it is instructive to define and calculate the equal-time density responses as

$$\chi_{\mu\nu}(\mathbf{r},\mathbf{r}')=-\frac{1}{k_BT}\frac{\delta n_\mu(\mathbf{r})}{\delta\ln z_\nu(\mathbf{r}')}$$
$$=-[n_\mu n_\nu h_{\mu\nu}(\mathbf{r},\mathbf{r}')+n_\mu\delta_{\mu\nu}\delta(\mathbf{r}-\mathbf{r}')]/k_BT . \quad (14)$$

The latter expression assumes that μ or ν is a classical particle (i.e., an ion). The density responses are connected with the direct correlations via

$$\frac{n_\nu}{k_BT}\delta_{\mu\nu}\delta(\mathbf{r}-\mathbf{r}')+\chi_{\mu\nu}(\mathbf{r},\mathbf{r}')$$
$$=n_\nu\sum_\lambda\int d\mathbf{r}_1\chi_{\mu\lambda}(\mathbf{r},\mathbf{r}_1)c_{\lambda\nu}(\mathbf{r}_1,\mathbf{r}') . \quad (15)$$

Since the system under investigation is homogeneous, a two-point function such as those in Eq. (15) depends only on differences in the spatial coordinates. The Fourier transform of Eq. (14) with respect to the differences gives the static density response, which in turn is expressed[1,2] in terms of $\chi_\mu^{(0)}(k,0)$ and $G_{\mu\nu}(k)$.

The electron-screened ion-ion potential is thus calculated as

$$u_{22}(k)=v_{22}(k)/\varepsilon_{22}^e(k) , \quad (16)$$

where $v_{22}(k)=4\pi e^2/k^2$ and

$$\frac{1}{\varepsilon_{22}^e(k)}=1+\frac{v_{11}(k)[1-G_{12}(k)]^2\chi_1^{(0)}(k,0)}{1-v_{11}(k)[1-G_{11}(k)]\chi_1^{(0)}(k,0)} . \quad (17)$$

Analogously, the electron-screened ion-ion direct correlation function is given by

$$d_{22}(k)=c_{22}(k)+\frac{1}{n_2}\frac{v_{12}^2(k)[1-G_{12}(k)]^2\chi_1^{(0)}(k,0)\chi_2^{(0)}(k,0)}{1-v_{11}(k)[1-G_{11}(k)]\chi_1^{(0)}(k,0)} . \quad (18)$$

The HNC equations now read as

$$g_{22}(r)=\exp[-u_{22}(r)/k_BT+h_{22}(r)-d_{22}(r)] , \quad (19)$$

$$h_{22}(k)=d_{22}(k)+n_2h_{22}(k)d_{22}(k) , \quad (20)$$

The ion-ion LFC and static structure factor are calculated as

$$G_{22}(k)=\frac{1}{\varepsilon_{22}^e(k)}+\frac{k_BTd_{22}(k)}{v_{22}(k)}$$
$$=1+\frac{k_BTc_{22}(k)}{v_{22}(k)} , \quad (21)$$

$$S_{22}(k)=\frac{1}{1-n_2d_{22}(k)} . \quad (22)$$

Once an explicit formulation for $G_{11}(k)$ and $G_{12}(k)$ is obtained, we thus have a complete description of the interparticle correlations in the hydrogen plasma. In the following section, we shall formulate $G_{11}(k)$ and $G_{12}(k)$ in the MCA scheme.

IV. MCA SCHEME

We describe quantum-mechanical correlations between electrons and ions as well as between electrons by the MCA scheme, which was derived from a convolution approximation to the triple correlation functions.[6] The scheme predicted the thermodynamic properties accurately and self-consistently both for the classical OCP (Ref. 7) and for the electron liquid in the ground state.[8] We expect that it may likewise provide a useful tool in the analysis of the electrons at an arbitrary degeneracy.

Following the equation of motion for the density fluctuations,

$$\rho_\mu(\mathbf{k})=\sum_{j=1}^{N_\mu}\exp(-i\mathbf{k}\cdot\mathbf{r}_{\mu j}) ,$$

one derives a relation for the LFC as[8]

$$N_\mu\sum_\nu Z_\mu Z_\nu G_{\mu\nu}(k)\langle\rho_\nu(\mathbf{k})\rho_\lambda(-\mathbf{k})\rangle=-\sum_\nu\sum_{\mathbf{q}}{}' I(\mathbf{k},\mathbf{q})Z_\mu Z_\nu[\langle\rho_\mu(\mathbf{k}-\mathbf{q})\rho_\nu(\mathbf{q})\rho_\lambda(-\mathbf{k})\rangle-\langle\rho_\mu(\mathbf{k})\rho_\lambda(-\mathbf{k})\rangle\delta_{\mu\nu}] . \quad (23)$$

Here $I(\mathbf{k},\mathbf{q})=\mathbf{k}\cdot\mathbf{q}/q^2$, $\langle\ \rangle$ refers to a statistical average, the prime means omission of the terms with $\mathbf{q}=\mathbf{0}$ and $\mathbf{q}=\mathbf{k}$ in the $\mathbf{q}$ summation, and N_μ is the total number of μ particles. For the symmetry of interparticle forces between μ and λ,

we symmetrize Eq. (23) as

$$N_\mu \sum_\nu Z_\mu Z_\nu G_{\mu\nu}(k)\langle\rho_\nu(\mathbf{k})\rho_\lambda(-\mathbf{k})\rangle + N_\lambda \sum_\nu Z_\lambda Z_\nu G_{\lambda\nu}(k)\langle\rho_\nu(\mathbf{k})\rho_\mu(-\mathbf{k})\rangle$$
$$= \sum_\nu \sum_{\mathbf{q}}{}' I(\mathbf{k},\mathbf{q}) Z_\mu Z_\nu [\langle\rho_\mu(\mathbf{k}-\mathbf{q})\rho_\nu(\mathbf{q})\rho_\lambda(-\mathbf{k})\rangle - \langle\rho_\nu(\mathbf{k})\rho_\lambda(-\mathbf{k})\rangle\delta_{\mu\nu}]$$
$$- \sum_\nu \sum_{\mathbf{q}}{}' I(\mathbf{k},\mathbf{q}) Z_\lambda Z_\nu [\langle\rho_\lambda(\mathbf{k}-\mathbf{q})\rho_\nu(\mathbf{q})\rho_\mu(-\mathbf{k})\rangle - \langle\rho_\nu(\mathbf{k})\rho_\mu(-\mathbf{k})\rangle\delta_{\lambda\nu}] \ . \tag{24}$$

The triple correlation functions in Eq. (24) are factored in the convolution approximation[1,6,8] as

$$\langle\rho_\mu(\mathbf{k}-\mathbf{q})\rho_\nu(\mathbf{q})\rho_\lambda(-\mathbf{k})\rangle \approx \sum_\eta \left[\frac{N_\mu N_\nu N_\lambda}{N_\eta}\right]^{1/2} S_{\mu\eta}(|\mathbf{k}-\mathbf{q}|)S_{\nu\eta}(q)S_{\lambda\eta}(k) \ , \tag{25}$$

where $S_{\mu\nu}(k)=\langle\rho_\mu(\mathbf{k})\rho_\nu(-\mathbf{k})\rangle/\sqrt{N_\mu N_\nu}$ is the static structure factor. We thus find from Eq. (24)

$$G_{11}(k)=\frac{1}{2N_1}\sum_{\mathbf{q}}{}' \left[K(\mathbf{k},\mathbf{q})[1+\bar{S}_{11}(q)]+I(\mathbf{k},\mathbf{q})\frac{Z_2}{Z_1}\left[\frac{n_2}{n_1}\right]^{1/2}\bar{S}_{12}(q)\right][S_{11}(|\mathbf{k}-\mathbf{q}|)-1]$$
$$-\frac{1}{2N_1}\sum_{\mathbf{q}}{}' J(\mathbf{k},\mathbf{q})\frac{Z_2}{Z_1}\left[\frac{n_2}{n_1}\right]^{1/2}[1+\bar{S}_{11}(q)]S_{12}(|\mathbf{k}-\mathbf{q}|)$$
$$-\frac{1}{N_1}B_{12}(k)\sum_{\mathbf{q}}{}' \left\{I(\mathbf{k},\mathbf{q})\frac{Z_2}{Z_1}[\bar{S}_{22}(q)-\bar{S}_{11}(q)]S_{12}(|\mathbf{k}-\mathbf{q}|)\right.$$
$$\left.+\tfrac{1}{2}K(\mathbf{k},\mathbf{q})\left[\left[\frac{n_1}{n_2}\right]^{1/2}-\frac{Z_2^2}{Z_1^2}\left[\frac{n_2}{n_1}\right]^{1/2}\right]\bar{S}_{12}(q)S_{12}(|\mathbf{k}-\mathbf{q}|)\right\} , \tag{26}$$

$$G_{12}(k)=-\frac{1}{2\sqrt{N_1N_2}}C(k)\sum_{\mathbf{q}}{}' K(\mathbf{k},\mathbf{q})\bar{S}_{12}(q)S_{12}(|\mathbf{k}-\mathbf{q}|)$$
$$-\frac{1}{2\sqrt{N_1N_2}}B_{11}(k)\sum_{\mathbf{q}}{}' \{I(\mathbf{k},\mathbf{q})[1+\bar{S}_{11}(q)]S_{12}(|\mathbf{k}-\mathbf{q}|)+J(\mathbf{k},\mathbf{q})\bar{S}_{12}(q)[S_{11}(|\mathbf{k}-\mathbf{q}|)-1]\}$$
$$-\frac{1}{2\sqrt{N_1N_2}}B_{22}(k)\sum_{\mathbf{q}}{}' \{I(\mathbf{k},\mathbf{q})[1+\bar{S}_{22}(q)]S_{12}(|\mathbf{k}-\mathbf{q}|)+J(\mathbf{k},\mathbf{q})\bar{S}_{12}(q)[S_{22}(|\mathbf{k}-\mathbf{q}|)-1]\} \ . \tag{27}$$

Here $J(\mathbf{k},\mathbf{q})=\mathbf{k}\cdot(\mathbf{k}-\mathbf{q})/|\mathbf{k}-\mathbf{q}|^2$, $K(\mathbf{k},\mathbf{q})=I(\mathbf{k},\mathbf{q})+J(\mathbf{k},\mathbf{q})$, and

$$B_{\mu\nu}(k)=S_{\mu\nu}(k)/[S_{11}(k)+S_{22}(k)] \ , \tag{28}$$

$$C(k)=B_{11}(k)\left[\frac{n_2}{n_1}\right]^{1/2}\frac{Z_2}{Z_1}+B_{22}(k)\left[\frac{n_1}{n_2}\right]^{1/2}\frac{Z_1}{Z_2} \ . \tag{29}$$

In Eqs. (26) and (27), we have classified the contributions of the structure factors physically into two parts: fluctuations and screening. The structure factors acting as screening functions[6-8] have been designated in these equations by $\bar{S}_{\mu\nu}(k)$, and are parametrized as

$$\bar{S}(k)=\frac{k^2}{k^2+k_0^2} \ , \tag{30}$$

$$\bar{S}_{11}(k)=\frac{k^2+k_1^2}{k^2+k_{01}^2} \ , \tag{31}$$

$$\bar{S}_{22}(k)=\frac{k^2+k_2^2}{k^2+k_{02}^2} \ , \tag{32}$$

$$\bar{S}_{12}(k)=\tfrac{1}{2}[\bar{S}_{11}(k)+\bar{S}_{22}(k)]-\bar{S}(k) \ . \tag{33}$$

The parameters k_0, k_1, k_{01}, k_2, k_{02} are determined so that the thermodynamic consistency conditions,

$$\sum_{\mathbf{k}} v(k)[\bar{S}_{\mu\nu}(k)-\delta_{\mu\nu}]=\sum_{\mathbf{k}} v(k)[S_{\mu\nu}(k)-\delta_{\mu\nu}] \ , \tag{34}$$

$$\bar{S}_{\mu\nu}(0)=S_{\mu\nu}(0) \ , \tag{35}$$

are met.

With such a modification of the screening functions, ensuring thermodynamic consistency, $G_{\mu\nu}(k)$ in Eqs. (26) and (27) are expressed in forms linear with respect to the unknown functions $S_{\mu\nu}(k)$. The latter functions, in turn, can be expressed as functionals of $G_{\mu\nu}(k)$ via the fluctuation-dissipation theorem. We have thus obtained the HNC MCA set of integral equations for the calculations of $S_{\mu\nu}(k)$ and $G_{\mu\nu}(k)$.

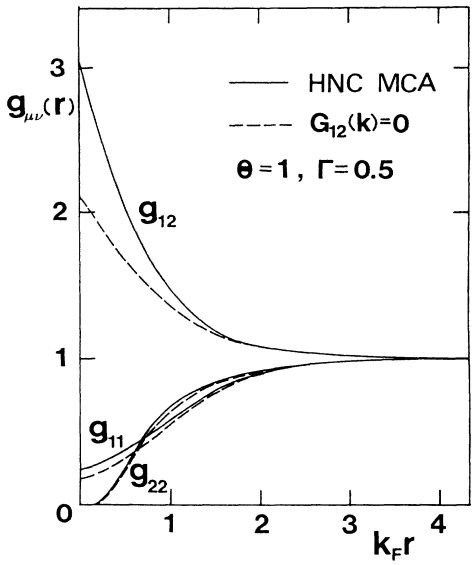

FIG. 2. Radial distribution functions.

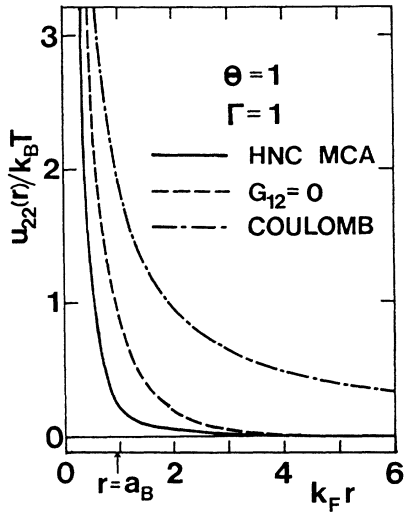

FIG. 4. Effective ion-ion potentials, as compared with the bare Coulomb potential (chain line).

V. CORRELATION FUNCTIONS

On the basis of the HNC MCA scheme developed in the preceding sections, we calculate the correlation functions in hydrogen plasmas though numerical solution to the integral equations by iteration. The method of solution is similar to those found in the literature.[9,12]

In Fig. 2, the results for $g_{\mu\nu}(r)$ are shown at $\Theta=1$ and $\Gamma=0.5$. For comparison, we also calculate $g_{\mu\nu}(r)$ in the HNC MCA scheme where $G_{12}(k)=0$ is set *a priori* and show the results in the figure. We observe that $G_{12}(k)$ acts to increase the values of $g_{\mu\nu}(r)$ in the short-range regime, implying physically an enhancement of attraction between the ions and the electrons.

The local-field corrections are likewise shown in Fig. 3 for a number of combinations between Θ and Γ. Note that $G_{11}(k)\geq 0$, $G_{22}(k)\geq 0$, and $G_{12}(k)\leq 0$. This fact implies that the differences between the effective potentials $v_{\mu\nu}(k)[1-G_{\mu\nu}(k)]$ and the bare potentials $v_{\mu\nu}(k)$ are *always* negative (i.e., attractive). In the strong-coupling regime, the magnitude of $G_{12}(k)$ remarkably increases in the large-k domain, leading to enhancement of the effective electron-ion attraction at short distances (cf. Fig. 2) and thereby to incipient bound states.

In Fig. 4, we plot the values of the effective ion-ion potential together with those with $G_{12}(k)=0$, and compare them with the bare Coulomb potential. We find that $G_{12}(k)$ acts to reduce the repulsive interionic potential in the short-range regime, leading to enhancement of $g_{22}(r)$. The short-range enhancement of $g_{11}(r)$, shown in Fig. 5, can likewise be interpreted in terms of reduction in the repulsive inter-electronic potential.

Figures 6 and 7 contain comparison with the DP results.[9] The DP ion-ion correlations, relying on the HNC approximation, resemble the HNC MCA result with $G_{12}(k)=0$, as one would have anticipated. It may be somewhat surprising at first to find in Fig. 7 that the DP scheme, assuming $G_{12}(k)=0$, appears capable of predict-

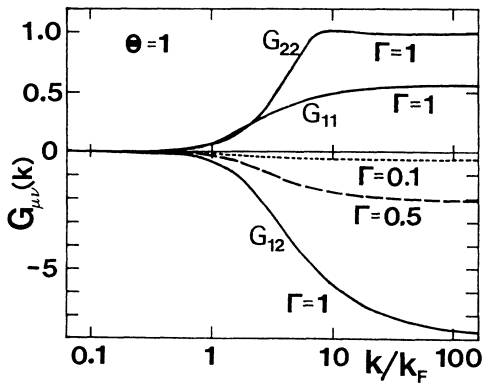

FIG. 3. Local-field corrections at $\Theta=1$ and $\Gamma=1$. For $G_{12}(k)$, the results at $\Gamma=0.1$ (dotted line) and $\Gamma=0.5$ (dashed line) are also plotted.

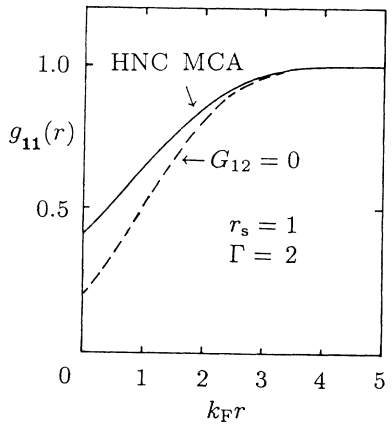

FIG. 5. Radial distribution functions between electrons.

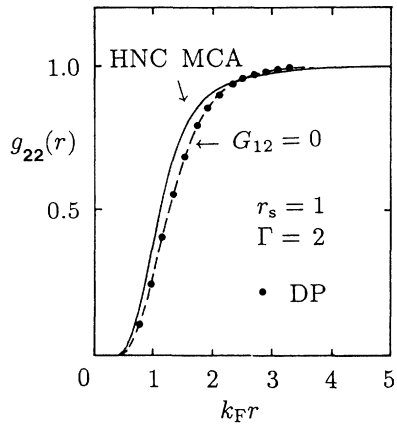

FIG. 6. Radial distribution functions between ions. Solid circles are the values obtained in Ref. 9.

ing an incipient bound state as is the present HNC MCA scheme with $G_{12}(k)$ fully taken into account. This feature can be attributed to the use in the DP scheme of the Kohn-Sham equation[10,14] for the electron-ion correlations (albeit with assumption $F_{12}^{\rm corr}=0$ in the LDA).

A salient demonstration of the incipient bound states in hydrogen plasmas predicted in the HNC MCA scheme is exhibited in Fig. 8, where the values of $g_{12}(0)$ are plotted as functions of Γ at $\Theta=1$. We here observe that the HNC MCA values approach asymptotically the isolated-atom values, Eq. (6), as the Coulomb coupling parameter increases.

VI. EQUATION OF STATE

With the knowledge of the structure factors, the interaction energy is calculated as

$$\frac{E_{\rm int}}{N}=\frac{1}{2}\sum_{\mu,\nu}\int d\mathbf{k}\frac{1}{(2\pi)^3}v_{\mu\nu}(k)[S_{\mu\nu}(k)-\delta_{\mu\nu}]\ , \tag{36}$$

where N denotes the total number of the electrons (or the ions). In Table I, we list the numerical results of the

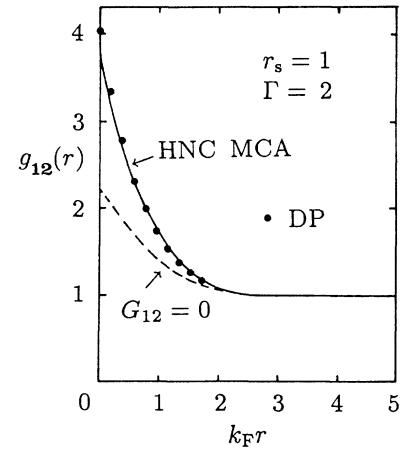

FIG. 7. Radial distribution functions between electrons and ions. Solid circles are the values obtained in Ref. 9.

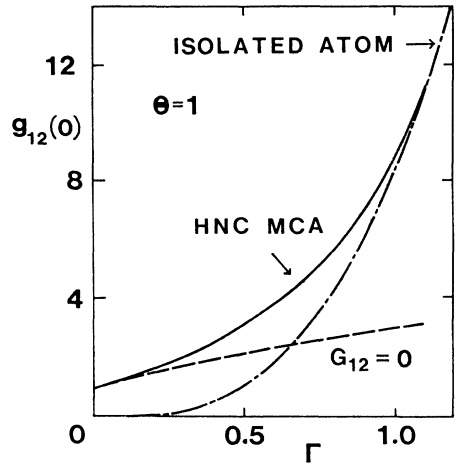

FIG. 8. Values of the electron-ion radial distribution function at $r=0$ as a function of Γ at $\Theta=1$. The corresponding quantity for a hydrogen atom is designated as an isolated atom.

computation for various parametric combinations of Θ and Γ.

In order to single out the difference between the present HNC MCA results and the previous IMTY results, we define

$$\delta\equiv\frac{E_{\rm int}-E_{\rm int}^{\rm IMTY}}{E_{\rm int}^{\rm IMTY}} \tag{37}$$

and exhibit their values on Fig. 1. For a given Θ, the HNC MCA results agree with the IMTY results at small values of Γ. As Γ increases, however, the HNC MCA prediction starts to deviate significantly from the IMTY prediction, due to incipient bound states which act to modify $g_{12}(r)$.

In Fig. 9, we plot $E_{\rm int}/Nk_BT$ calculated in the HNC MCA and IMTY schemes as functions of Γ. We here observe again that the HNC MCA prediction approaches asymptotically the isolated-atom value of Eq. (7) as Γ increases, another demonstration of an incipient bound-state effect. The IMTY results,[3] being proportional to $\Gamma^{3/2}$ for large Γ, predict a substantially smaller magnitude for the absolute value of the interaction energy near the metal-insulator boundaries. These new features should affect the nature of metal-insulator transition in dense hydrogen significantly.

For convenience in practical applications, we set

$$E_{\rm int}=E_{\rm int}^{\rm IMTY}+\Delta E_{\rm int}^{\rm SC} \tag{38}$$

and seek for a parametrized expression of the strong-coupling term, $\Delta E_{\rm int}^{\rm SC}$, with the result:

$$-\frac{\Delta E_{\rm int}^{\rm SC}}{N(e^2/a)}=\frac{a(\Theta)\Gamma+b(\Theta)\Gamma^2}{1+c(\Theta)\Gamma}\ , \tag{39}$$

$$a(\Theta)=\frac{0.0190\Theta}{1+2.2110\Theta}\ , \tag{40}$$

$$c(\Theta)=\frac{0.4444\Theta}{1+1.3078\Theta}\ , \tag{41}$$

$$b(\Theta)=1.8416\Theta c(\Theta)\ . \tag{42}$$

The former term, $E_{\rm int}^{\rm IMTY}$, has been accurately parametrized in Ref. 3. We note that the strong-coupling part, Eq. (39), of the interaction energy vanishes in the weak-coupling limit ($\Gamma \ll 1$) as it should. In the strong-coupling limit, Eq. (39) approaches $1.8416\Gamma\Theta$, which coincides with Eq. (7). The total energy, Eq. (38), reproduces all the values listed in Table I within 10%.

Once an explicit expression for the interaction energy is found, one can proceed to calculate other thermodynamic quantities such as the free energy and the pressure in the same way as in the previous studies.[1,3] The isothermal compressibility κ_T is defined and calculated as

$$\frac{1}{\kappa_T} \equiv -V\left[\frac{\partial P}{\partial V}\right]_{T,N_1,N_2} . \tag{43}$$

TABLE I. Interaction energy and the generalized Coulomb logarithms at various combinations of Θ and Γ.

Θ	Γ	$-E_{\rm int}/N(e^2/a)$	L_E	L_T
10	0.05	0.544 83	2.732	2.363
10	0.1	0.756 12	2.710	2.256
10	0.2	1.0918	3.295	2.557
10	0.3	1.5293	5.250	3.784
10	0.35	1.9768	8.041	5.573
5	0.1	0.750 09	2.097	1.725
5	0.2	1.0384	2.161	1.680
5	0.3	1.3024	2.506	1.853
5	0.4	1.6297	3.249	2.294
5	0.5	2.1899	5.002	3.384
1	0.1	0.756 99	0.9560	0.7507
1	0.2	0.959 78	0.8109	0.6047
1	0.3	1.1065	0.7482	0.5381
1	0.4	1.2285	0.7184	0.5024
1	0.5	1.3380	0.7073	0.4836
1	0.6	1.4417	0.7090	0.4758
1	0.7	1.5442	0.7214	0.4767
1	0.8	1.6492	0.7438	0.4853
1	0.9	1.7603	0.7775	0.5021
1	1.0	1.8822	0.8273	0.5301
1	1.1	2.0272	0.9144	0.5828
0.271 51	0.2	0.900 76	0.2314	0.1657
0.271 51	0.6	1.1755	0.1658	0.1106
0.271 51	1.0	1.3345	0.1448	0.093 25
0.271 51	1.6	1.5181	0.1341	0.084 02
0.271 51	1.8	1.5751	0.1336	0.083 28
0.271 51	2.0	1.6327	0.1345	0.083 50
0.271 51	2.4	1.7568	0.1421	0.087 89
0.271 51	2.5	1.7927	0.1466	0.090 61
0.1	0.5	1.0237	4.618×10^{-2}	2.879×10^{-2}
0.1	0.543 01	1.0401	4.496×10^{-2}	2.798×10^{-2}
0.1	1.0	1.1662	3.679×10^{-2}	2.259×10^{-2}
0.1	1.6290	1.2741	3.153×10^{-2}	1.914×10^{-2}
0.1	2.0	1.3227	2.971×10^{-2}	1.795×10^{-2}
0.1	2.7151	1.4014	2.752×10^{-2}	1.651×10^{-2}
0.1	3.0	1.4295	2.696×10^{-2}	1.614×10^{-2}
0.1	3.2581	1.4540	2.657×10^{-2}	1.588×10^{-2}
0.1	4.0	1.5215	2.594×10^{-2}	1.544×10^{-2}
0.1	4.3441	1.5523	2.587×10^{-2}	1.538×10^{-2}
0.1	5.0	1.6119	2.612×10^{-2}	1.551×10^{-2}
0.1	5.4301	1.6528	2.663×10^{-2}	1.580×10^{-2}
0.01	5.4301	1.2623	7.062×10^{-4}	4.130×10^{-4}
0.01	10.0	1.3290	5.776×10^{-4}	3.377×10^{-4}
0.01	16.290	1.3857	5.016×10^{-4}	2.932×10^{-4}
0.01	27.151	1.4582	4.505×10^{-4}	2.633×10^{-4}
0.01	30.0	1.4753	4.450×10^{-4}	2.601×10^{-4}
0.01	38.011	1.5222	4.415×10^{-4}	2.580×10^{-4}
0.01	43.441	1.5543	4.483×10^{-4}	2.619×10^{-4}

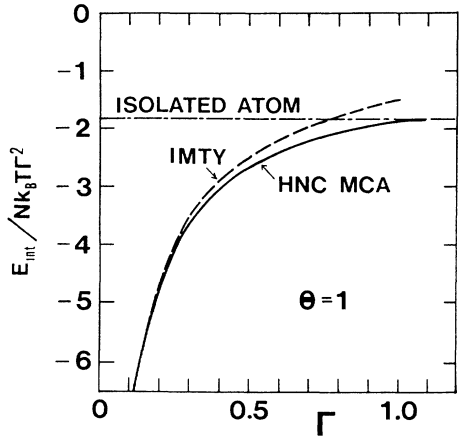

FIG. 9. Same as Fig. 8 for the normalized interaction energy, $E_{\rm int}/Nk_BT$.

The same quantity can be calculated via the compressibility sum rule[1] as

$$\frac{1}{\kappa_T}=\frac{1}{\kappa_T^0}-nk_BT(\gamma_{11}-2\gamma_{12}+\gamma_{22}) , \tag{44}$$

where

$$\gamma_{\mu\nu}=\frac{4\pi ne^2}{k_BT}\lim_{k\to 0}\frac{G_{\mu\nu}(k)}{k^2} \tag{45}$$

and κ_T^0 refers to the ideal-gas contribution to the isothermal compressibility. Figure 10 plots the values of κ_T^0/κ_T computed in two ways: (43) and (44). We note that the compressibility sum rule is violated in a large Γ regime, due mainly to the use of the HNC approximation for the ion-ion correlations. We also find in Fig. 10 that the values of κ_T may tend to diverge as Γ further increases. A question that remains to be investigated is if there exists any physical connection between such a thermodynamic instability and an eventual approach to an insulator phase.

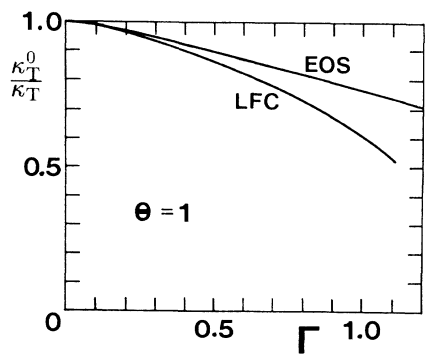

FIG. 10. Isothermal compressibility: EOS from Eq. (43), and LFC from Eq. (44).

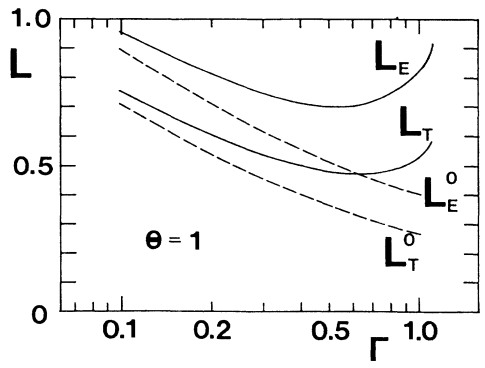

FIG. 11. Generalized Coulomb logarithms. L_E^0 and L_T^0 are those in the IMTY theory (Ref. 4).

VII. CONDUCTIVITIES

On the basis of the quantum-mechanical transport equations for the electrons, we have derived the expressions for the electric conductivity σ and the thermal conductivity κ as[1]

$$\frac{1}{\sigma}=4\left[\frac{2\pi}{3}\right]^{1/2}\frac{\Gamma^{3/2}}{\omega_p}L_E , \tag{46}$$

$$\frac{1}{\kappa}=\frac{52(6\pi)^{1/2}}{75}\frac{e^2}{k_B^2}\frac{\Gamma^{3/2}}{\omega_p}L_T . \tag{47}$$

Here $\omega_p=(4\pi ne^2/m)^{1/2}$ is the plasma frequency of the electrons, L_E and L_T are the generalized Coulomb logarithms given by

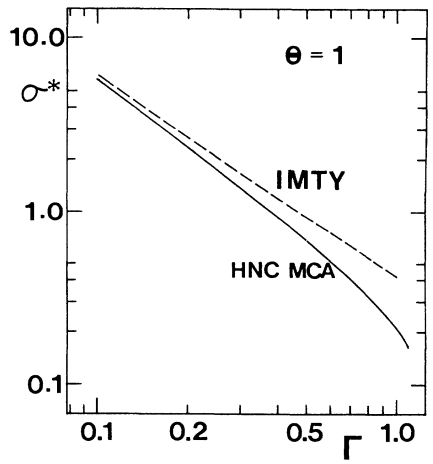

FIG. 12. Electric conductivity.

$$L_E=\frac{3\sqrt{\pi}\Theta^{3/2}}{4}\int_0^\infty dk\frac{1}{k}f_0(k/2)\frac{S_{22}(k)}{|\tilde{\varepsilon}(k)|^2}[1-G_{12}(k)]\ , \tag{48}$$

$$L_T=\frac{75\sqrt{\pi}\Theta^{9/2}}{104\Sigma^2}\int_0^\infty dk\frac{1}{k}\frac{S_{22}(k)}{|\tilde{\varepsilon}(k)|^2}[1-G_{12}(k)] \times\int_{k/2k_F}^\infty dx x(x^2-\lambda)^2\frac{\partial f_0(k_F x)}{\partial\alpha}\ . \tag{49}$$

In Eqs. (48) and (49),

$$f_0(k)=[\exp(\hbar^2k^2/2mk_BT-\alpha)+1]^{-1}\ , \tag{50}$$

$$\tilde{\varepsilon}(k)=1-v(k)[1-G_{11}(k)]\chi_1^{(0)}(k,0)\ , \tag{51}$$

$$\Sigma=\tfrac{7}{4}\frac{\Theta^{9/2}}{I_{1/2}(\alpha)}\{I_{5/2}(\alpha)I_{1/2}(\alpha)-\tfrac{25}{21}[I_{3/2}(\alpha)]^2\}\ , \tag{52}$$

$$\lambda=\tfrac{5}{3}\Theta\frac{I_{3/2}(\alpha)}{I_{1/2}(\alpha)}\ , \tag{53}$$

$$I_v(\alpha)=\int_0^\infty dz\frac{z^v}{\exp(z-\alpha)+1}\ . \tag{54}$$

The factor $1-G_{12}(k)$ in the Coulomb logarithms accounts for strong electron-ion coupling in scattering. It describes those short-range events where the electrons and ions, correlated strongly by the Coulombic attraction, scatter each other repeatedly. It thus represents an effect beyond the Born approximation and acts to enhance the values of the resistivities.

We have calculated L_E and L_T by substituting the HNC MCA values of $S_{\mu\nu}(k)$ and $G_{\mu\nu}(k)$ in Eqs. (48) and (49); the results are listed in Table I.

Figures 11–13 plot the values of the generalized Coulomb logarithms, the normalized electric and thermal conductivities ($\sigma^*=\sigma/\omega_p$ and $\kappa^*=\kappa/k_Bna^2\omega_p$), and

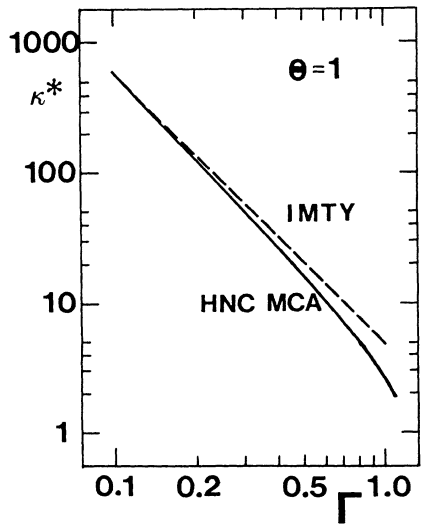

FIG. 13. Thermal conductivity.

TABLE II. Coefficients, p_k and q_k, in Eqs. (57) and (58) for L_E and L_T.

	L_E	L_T
p_2	0.27446	0.25826
p_3	−1.8486	−1.4523
p_4	10.577	7.2871
p_5	−11.187	−7.6455
p_6	3.2858	2.2151
q_1	2.0934	1.8900
q_2	−5.2431	−4.5398
q_3	14.159	13.639
q_4	−10.463	−10.367
q_5	3.7413	3.7272

compare them with the corresponding quantities in the IMTY theory.[4] We observe in Fig. 11 that L_E and L_T turn over at about $\Gamma=0.5$ and steeply increase thereafter, resulting in corresponding decreases in the conductivities (Figs. 12 and 13). Such a pronounced scattering rate in the large-Γ regime is a consequence of the strong attraction between the electrons and the ions brought about by the factor $1-G_{12}(k)$ in Eqs. (48) and (49); the steep increase in the resistivities should signal an approach to an insulator phase.

Again for convenience in practical applications, we set

$$L_{E(T)}=L^0_{E(T)}+\Delta L(\Gamma,\Theta) \tag{55}$$

and seek for a parametrized expression of the last term, with the result

$$\Delta L(\Gamma,\Theta)=\frac{p(\Theta)\Gamma^\alpha}{[1-q(\Theta)]^\beta}\ , \tag{56}$$

$$p(\Theta)=\frac{\sum_{k=2}^{6}p_k\Theta^k}{\sum_{k=0}^{6}\Theta^k}\ , \tag{57}$$

$$q(\Theta)=\frac{\sum_{k=1}^{5}q_k\Theta^k}{\sum_{k=0}^{5}\Theta^k}\ . \tag{58}$$

We have found $\alpha=0.5$ and $\beta=0.75$ from the behavior of ΔL in the small- and large-Γ regimes. The coefficients p_k and q_k are tabulated in Table II for L_E and L_T. With the IMTY values, L^0_E and L^0_T, parametrized in Ref. 4, Eq. (55) reproduces the values in Table I for $\Gamma\le5$ within 8% and 15% for L_E and L_T, respectively. At $r_s=1$ and $\Gamma=2$, the electric resistivity in the present HNC MCA theory is 2.76×10^{-5} Ω cm while that of DP calculation[11] gives 2.33×10^{-5} Ω cm. The latter authors used a phase-shift analysis in the calculation of scattering cross section for the electrons passing through average distribution of the ions.

VIII. CONCLUSION

We have presented a detailed HNC MCA theory of strongly coupled hydrogen plasmas, elucidating the role that the electron-ion LFC, $G_{12}(k)$, plays especially near the metal-insulator boundaries. A salient prediction of the theory is an emergence of Rydberg states or incipient bound states in the metallic phase, which significantly modifies the equation of state and acts to increase the resistivities.

ACKNOWLEDGMENTS

This research was supported in part through Grants-in-Aid for Scientific Research provided by the Ministry of Education, Science and Culture of Japan. The research by one of the authors (S.I.) was supported in part by the National Science Foundation under Grant No. PHY82-17853, supplemented by funds from the National Aeronautics and Space Administration.

[1]For a review, see S. Ichimaru, H. Iyetomi, and S. Tanaka, Phys. Rep. **149**, 91 (1987).

[2]For a general formalism, see S. Ichimaru, S. Mitake, S. Tanaka, and X.-Z. Yan, Phys. Rev. A **32**, 1768 (1985).

[3]For the equation of state, see S. Tanaka and S. Ichimaru, Phys. Rev. A **32**, 3756 (1985).

[4]For the conductivities, see S. Ichimaru and S. Tanaka, Phys. Rev. A **32**, 1790 (1985).

[5]D. Pines and P. Nozieres, *The Theory of Quantum Liquids* (Benjamin, New York, 1966), Vol. I.

[6]K. Tago, K. Utsumi, and S. Ichimaru, Prog. Theor. Phys. **65**, 54 (1981).

[7]X.-Z. Yan and S. Ichimaru, J. Phys. Soc. Jpn. **56**, 3853 (1987).

[8]S. Tanaka and S. Ichimaru, Phys. Rev. B **36**, 1036 (1989).

[9]M. W. C. Dharma-wardana and F. Perrot, Phys. Rev. A **26**, 2096 (1982).

[10]For a review, see W. Kohn and P. Vashishta, in *Theory of Inhomogeneous Electron Gas,* edited by S. Lundqvist and N. H. March (Plenum, New York, 1983).

[11]F. Perrot and M. W. C. Dharma-wardana, Phys. Rev. A **36**, 238 (1987).

[12]S. Tanaka and S. Ichimaru, J. Phys. Soc. Jpn. **55**, 2278 (1986).

[13]J.-P. Hansen and I. R. McDonald, *Theory of Simple Liquids,* 2nd ed. (Academic, London, 1986).

[14]W. Kohn and J. L. Sham, Phys. Rev. A **140**, 1133 (1965).